Detection of Jumps in Single-Channel Data Containing Subconductance Levels

Silke Draber and Roland Schultze
Institut für Angewandte Physik der Universität Kiel, D-24098 Kiel, Germany

ABSTRACT Detection algorithms are widely used for the analysis of single-channel data because they remove the background noise from the measured current signal and reconstruct the noise-free time series. Standard detection algorithms assume channels switching only between zero and full conductance. Many types of channels, however, show subconductance levels. A new detection algorithm for data containing sublevels, the so-called sublevel Hinkley-detector (SHD), calculates several test values in parallel, one for each possible jump. The velocity of increase has a maximum for the correct jump. This feature is used to detect the jump and to diagnose the new level of current. Because patch-clamp data are always filtered by an antialiasing low-pass filter before sampling, the algorithm is supplemented by a special diagnosis phase accounting for the distortion of the originally rectangular jumps. Along with the reconstructed (noise-free) time series the SHD also gives a matrix of the transition counts between the levels. This matrix is a useful statistical tool for the decision whether the observed channel(s) have in fact a subconductance conformation or if there are simply several channels of different conductivity contained within the patch.

INTRODUCTION

A detector analyzes the noisy experimental time series and reconstructs the noise-free original time series of open and closed events, i.e., it detects the jumps of the current signal. Standard methods for detecting jumps in patch-clamp data are the Bessel filter with threshold analysis (Colquhoun and Sigworth, 1983), the Hinkley-detector (Page, 1955; Hinkley, 1971; Basseville and Benveniste, 1986, Schultze and Draber, 1993), and the higher-order Hinkley-detector (Schultze and Draber, 1993). All these detection methods require prior knowledge about the levels of current between which the jumps of the current signal can occur. They work with equidistant current levels only.

A problem often encountered when analyzing patch-clamp data are levels of current that are not equally spaced. This can originate from channels of different conductivity within the patch or, as is physiologically more interesting, from channels with a molecular conformation of reduced conductivity, i.e., with a subconductance level (Patlak, 1988, 1993; Schild et al., 1991; Tyerman et al., 1992; Ferguson et al., 1993; Ramanan and Brink, 1993). Fig. 1 shows a record of a single channel that frequently reduces its conductivity to a subconductance level of about 55% of the full conductance. The amplitude histogram in Fig. 1 *B* shows a sublevel located between the large peaks of the baseline and the full current. All the standard detectors mentioned above cannot be applied to such data. There have been some approaches to deal with patch-clamp data containing sublevels. Tyerman et al. (1992) analyze plots showing the channel current versus its derivative. A similar method makes use of mean-variance plots (Patlak, 1988, 1993). Another technique is based on hidden Markov models (Chung et al., 1990).

In this article, we introduce the "sublevel Hinkley-detector" (SHD). The development of this detection algorithm is based on the so-called dynamic Hinkley-detector, which was originally invented for the online identification of technical processes (Schultze, 1992, 1993) where jumps to time-varying levels had to be detected. Now, we describe the application to the analysis of patch-clamp data containing sublevels. For this quite different purpose, the basic algorithm is modified, mainly by the introduction of a special diagnosis phase subsequent to jump detection.

Fig. 2 gives a preview of what the algorithm is capable of. The upper trace is the noisy data, a section of Fig. 1 *A*. The lower trace (Fig. 2 *B*) is the noise-free current signal reconstructed by the SHD.

THE ALGORITHM

A detector scans through the time series in an iterative way. It always assumes one level of current to be the actual level. For every new data point the detector tests whether the sampled value makes it likely that a jump to another level of current may have occurred. If the jump seems more likely than the actual level, the detector detects a jump. After detection it has to diagnose what type of jump has occurred. After jump detection and diagnosis, the detector goes on scanning through the current signal, but now with the new level as actual level.

Alternative levels

Fig. 3 illustrates the nomenclature of levels and of jump types. It displays a schematic time series of two channels switching between conformations of full (f), reduced (s), and zero conductance. The current signal switches between the levels $0f + 0s$, $1f + 0s$, $2f + 0s$, $0f + 1s$, $1f + 1s$, $0f + 2s$.

Received for publication 28 February 1994 and in final form 14 July 1994.
Address reprint requests to Dr. Silke Draber, Institut für Angewandte Physik der Universität Kiel, D-24098 Kiel, Germany. Fax: 49 431 880 4608; E-mail: pan05@rz.uni-kiel.d400.de.

0006-3495/94/10/1404/10 $2.00

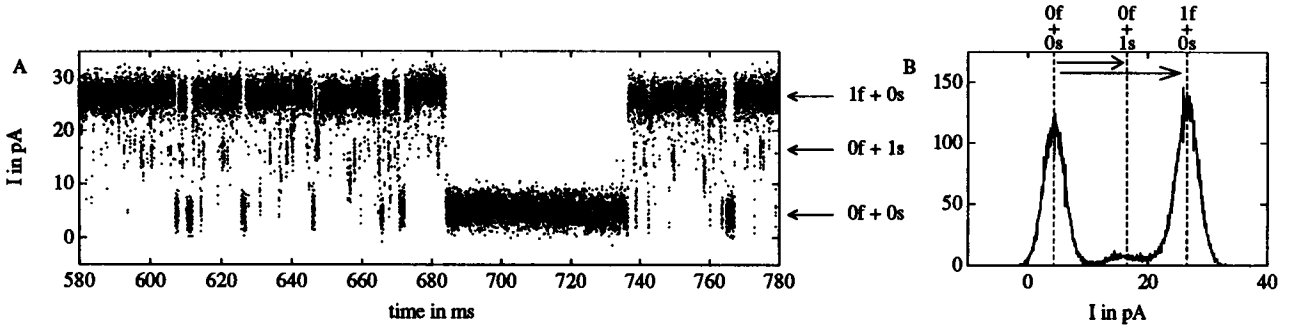

FIGURE 1 Current signal of a K^+ channel in an excised patch of the tonoplast of *Chara corallina* at 145.7 mV with symmetrical solutions (250 mM KCl, 5 mM $CaCl_2$). (*A*) Pipette current sampled at 100 kHz. The levels $0s + 0f$, $1s + 0f$, $0s + 1f$ are shown by the arrows on the right. The displayed data is a representative section (200 ms) of the whole record, which is 800 ms in length. (*B*) Amplitude histogram of the whole record with the noise-free levels as vertical dashed lines. The levels of current do not have equal distance. The arrows mark the full single-channel current $I_f = 22.2$ pA, and the subconductance current $I_s = 12.1$ pA.

The question arises, what alternative levels can be reached with one jump from a given level? Six principal types of jumps can be distinguished: a channel with full conductivity can open $(+f)$ or close $(-f)$, a subconductance or small channel can open $(+s)$ or close $(-s)$. If a transition between the subconductance and the full conductance states is possible in the gating scheme, a full conductance can change to a small conductance $(f \rightarrow s)$ and vice versa $(s \rightarrow f)$. Examples for these six jump types are shown in Fig. 3 as arrows. The *f/s* diagram (Fig. 4), where every level is represented by a box, provides a systematic approach. In most cases, all six types of jumps can occur from a given level, e.g., from level $1f + 2s$:

1) $1f + 2s \xrightarrow{+f} 2f + 2s$
2) $1f + 2s \xrightarrow{+s} 1f + 3s$
3) $1f + 2s \xrightarrow{-f} 0f + 2s$
4) $1f + 2s \xrightarrow{-s} 1f + 1s$
5) $1f + 2s \xrightarrow{f \rightarrow s} 0f + 3s$
6) $1f + 2s \xrightarrow{s \rightarrow f} 2f + 1s$

From some levels at the edge or corner of the *f/s* diagram in Fig. 4 there are only two, three, or four alternatives. Starting from the baseline leaves only two jump alternatives, $+f$ or $+s$, as shown in Fig. 4.

A detector for subconductance analysis has to detect if there is a jump from one level to another. After detection it has to diagnose which of the two, three, four, or six types of jumps has taken place.

Calculation of test values h_{ft} and jump detection

The classic Hinkley-detector (Hinkley, 1971; Basseville and Benveniste, 1986; Schultze and Draber, 1993) looking for a jump of the signal z_t from level μ_0 up to level μ_1 calculates the test value g:

$$g_t = g_{t-1} + (e_t - p) \qquad (1)$$

where $p = (\mu_1 - \mu_0)/2$ is the half absolute difference between two levels and $e_t = z_t - \mu_0$ denotes the innovation, the difference of the sampled value to the actually assumed level of current. The test values range between 0 and a threshold λ. If a test value falls below 0 it is immediately reset to 0.

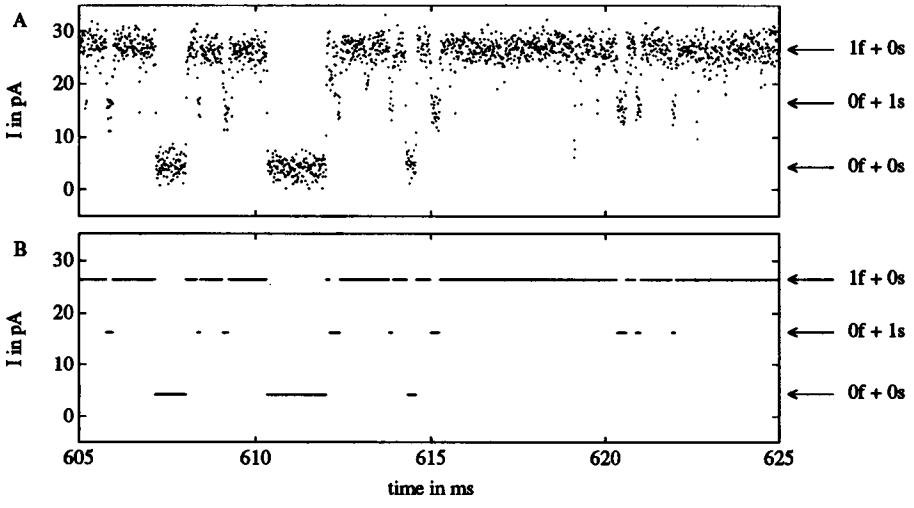

FIGURE 2 (*A*) A section (20 ms) of the time series in Fig. 1. This zoomed presentation gives a better impression of the frequent transitions between the full-conducting level $1f + 0s$ and the sublevel $0f + 1s$. (*B*) Noise-free time series of gating reconstructed by the SHD as developed in this article.

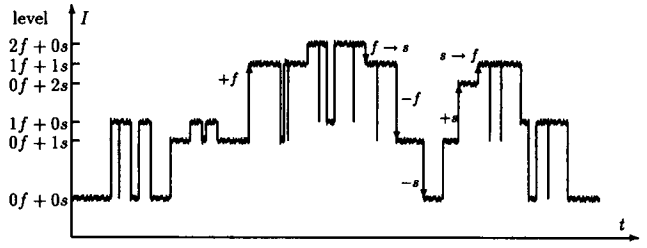

FIGURE 3 Schematic time series of current produced by two identical channels with full conductance (f) and subconductance (s). The level $0f + 0s$ is the baseline. There are six principal types of jumps. A full conductance can open ($+f$) or close ($-f$), a small conductance can open ($+s$) or close ($-s$), or a full conductance can convert to a small one ($f \rightarrow s$) or vice versa ($s \rightarrow f$). Examples of these jump types are shown as upward or downward arrows.

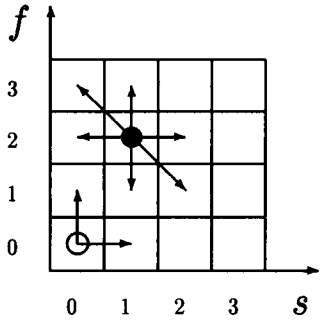

FIGURE 4 Alternative levels in the f/s diagram. From most of the levels, e.g., $2f + 1s$ (●), all six types of jumps (see Fig. 3) are possible. The six arrows starting at $2f + 1s$ (●) show to which alternative levels the current signal can jump from there. From some levels at the edges of the f/s diagram, there are fewer than six transitions possible. An important example often referred to in this article is the baseline $0f + 0s$ (○). The two types of jump, one to the full-conducting level $1f + 0s$ and one to the sublevel $0f + 1s$, are again shown as arrows.

If a test value rises and exceeds the detection threshold λ, the Hinkley-detector detects a jump. For details, see Schultze and Draber (1993).

In contrast, the new SHD makes use of many "half jump magnitudes" p_i to account for the different alternative levels. The innovation term $(e_t - p_i)$ is multiplied with the half jump magnitude p_i to construct a bank of test values h_{it}, one for each jump i:

$$h_{it} = h_{i,t-1} + p_i \cdot (e_t - p_i) \qquad (2)$$

A jump is detected when one test value h_{it} reaches the threshold ϵ. The choice of ϵ is addressed below.

The SHD finds the correct candidate by virtue of a peculiar dependence of the speed of growth of the test values on p_i. The difference $p_i \cdot (e_t - p_i)$ between the subsequent test values in Eq. 2 is the speed of growth, i.e., the slope of the time series of test values (Fig. 5).

Assume a true jump to a level lying $2 \cdot p_w$ away from the actual level. p_w is the true half jump magnitude. Neglecting the noise, the innovation becomes $e_t = 2 \cdot p_w$ after the jump. The speed of growth is

$$h_{i,t} - h_{i,t-1} = p_i(e_t - p_i) = p_i(2p_w - p_t). \qquad (3)$$

This is a parabola (Fig. 6), which has its maximum at $p_i = p_w$. This result ensures that the test value for the true jump has the strongest increase and therefore reaches the threshold first. If the true new level is not in the set of alternative levels, the SHD selects the one closest to the true jump magnitude (see Discussion).

Details of the algorithm

The details of the algorithm are illustrated by the examples shown in Fig. 5. The detector must decide whether the jump from the baseline goes to the full level $e_t \approx 2p_1$ or to the sublevel $e_t \approx 2p_2$. The series of test values are displayed as circles. Full circles represent the test values h_{1t} related to a jump to the full level, and open circles represent the test values h_{2t} indicating a jump to the sublevel.

In Fig. 5, A and B, the innovation e_t before the jump is 0 because there is no noise. Fig. 5, C and D, shows the scattering of the innovation due to noise. Before a jump, the slope $p_i \cdot (e_t - p_i)$ in Eq. 2 is negative. In a linear detector, this would lead to a decrease of the test values h_{it}. To keep the algorithm always alert, a test value h_{it} is immediately reset to 0 if it becomes negative. This is the inherent nonlinearity of the detector.

After the jump, both test values in Fig. 5, A and B, increase linearly. In Fig. 5, A and C, the test value h_{1t} for the full level increases faster than the test value h_{2t} for the sublevel and therefore reaches the threshold ϵ for jump detection earlier. Thus, the SHD detects the jump to the full conductance level, which is actually correct. In Fig. 5, B and D, the true jump is an opening of a subconducting channel. In that situation the test value h_{2t} for the jump $+s$ reaches the threshold ϵ first. A jump to the sublevel is detected correctly.

One important observation in the examples with background noise (Fig. 5, C and D) is that the noise has little influence on the general behavior of the test values. The increasing test values are quite insensitive to noise because they are calculated as cumulative sums (Eq. 2). Positive and negative deviations from the mean cancel each other out.

Generally, if a test value h_{it} exceeds the threshold ϵ, a jump to the corresponding level l_i is detected. If two or more test values cross the threshold within the same sampling interval, the diagnosis selects the greatest one.

After a jump to the new level l_i has been detected, the time of the jump is estimated (backward) to be the last sampling step with $h_{it} = 0$. In the examples of Fig. 5, the times of the jump would have been estimated correctly. After detection and diagnosis all test values are reset to 0 and the algorithm starts from the estimated jump moment with the new level l_i as actual level.

Choice of the threshold

In the absence of noise, as in Fig. 5, A and B, it would be sufficient to choose any small value as threshold ϵ. In the presence of noise, the threshold ϵ has to be chosen according to the noise. The aim is to select ϵ as small as possible without having too many false alarms. As a rule,

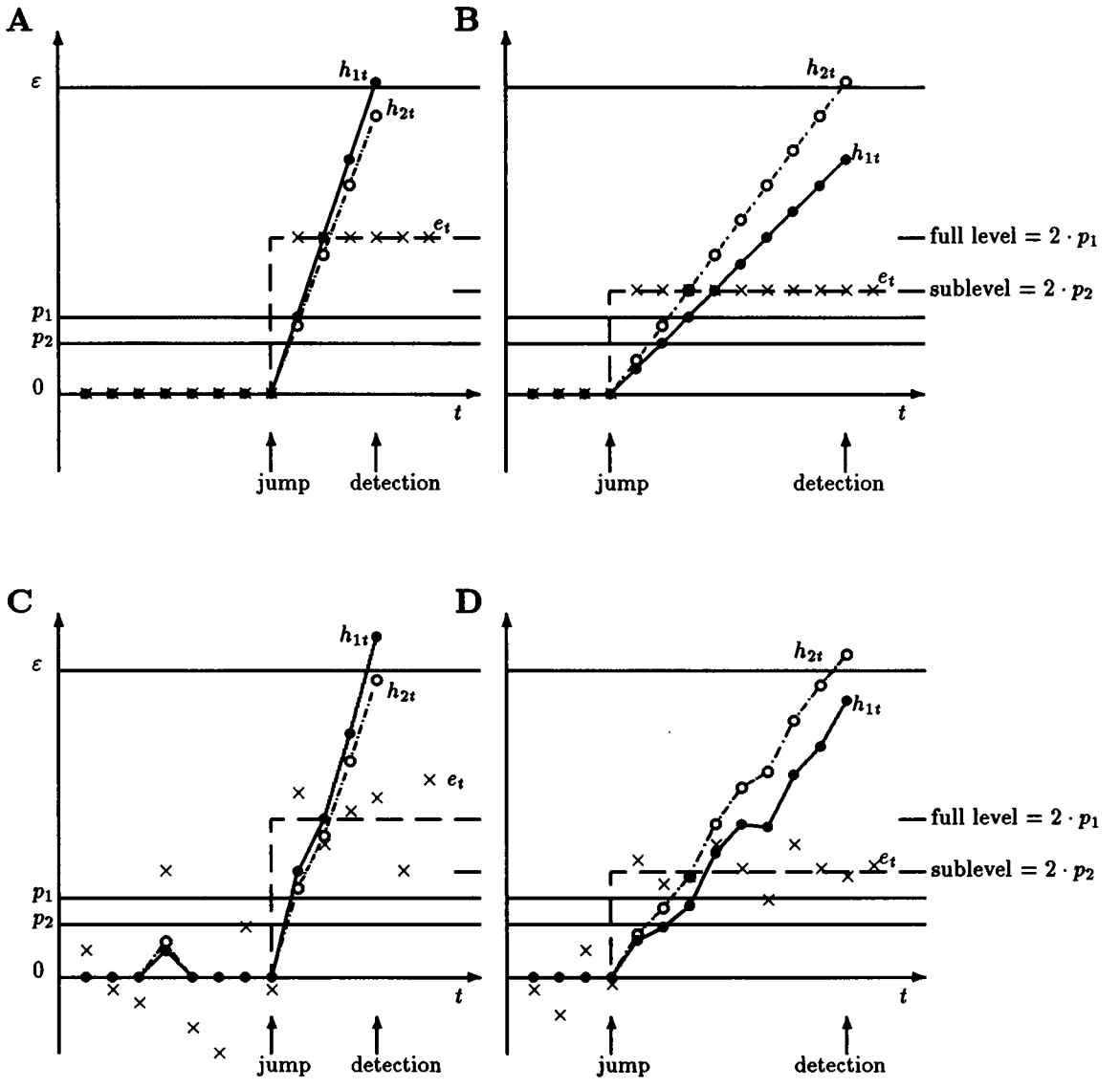

FIGURE 5 Detection of jumps from the baseline $0f + 0s$ to the full conductance level $1f + 0s$ or to the subconductance level $0f + 1s$. In this plot the actual level before the jump is arbitrarily chosen to be 0. This is done without loss of generality because the innovation e_t (×) and the jump magnitudes $2p_1$ and $2p_2$ are defined as differences to the actual level. The broken line shows the idealized jump of the mean value of the current. The detector has to decide whether the jump from the baseline goes to the full level with jump magnitude $2p_1$ or to the sublevel with jump magnitude $2p_2$. The series of test values are displayed as circles, ● for the test values h_{1t} that indicate a jump to the full level, and ○ for the test values h_{2t} indicating a jump to the sublevel. At the beginning, before the jump has occurred, both test values often have identical value 0. (*A*) A noise-free jump from the baseline to the full level. After the jump, both test values begin to rise. Four sampling steps later the test value h_{1t} crosses the threshold ϵ. The jump is detected and diagnosed to have gone to the full level. (*B*) A noise-free jump to the sublevel. Here the test values do not rise as fast as in (A). It takes nine sampling steps until the jump to the sublevel is detected. (*C, D*) With noise: the innovation values (×) scatter around their mean value, 0 before the jump and $2p_1$ or $2p_2$ afterward. As in the noise-free cases, the test value for the correct alternative level increases faster than the other test value and therefore reaches the threshold ϵ for jump detection earlier. Scales: to show the test values h_{it} (dimension A^2) and the current values e_t (dimension A) in the same plot, the scaled quantities h_{it}/p_1 and ϵ/p_1 are used.

ϵ is chosen proportional to the variance σ^2 of the background noise.

$$\epsilon = 8 \cdot \sigma^2 \tag{4}$$

This rule is deduced by correspondence to the standard Hinkley-detector whose false alarm rate has been thoroughly studied before (Schultze and Draber, 1993). To have fewer than 100 false alarms per 1,000,000 sampling steps, the threshold λ of the Hinkley-detector is chosen according to the signal-to-noise ratio (SNR)

$$SNR^2 \cdot \lambda/p = 32 \tag{5}$$

$$\left(\frac{2p}{\sigma}\right)^2 \lambda \Big/ p = 32 \tag{6}$$

$$p\lambda = 8\sigma^2 \tag{7}$$

According to the multiplication with p_i in Eq. 2, $p\lambda$ corresponds to ϵ. Thus, Eq. 7 leads to the rule for the SHD, given in Eq. 4.

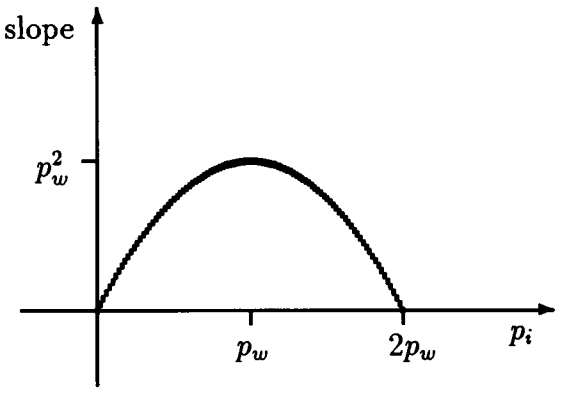

FIGURE 6 The slope of the increasing test value h_{it} versus the assumed half jump magnitude p_i (Eq. 3). The test value increases the stronger, the closer the assumed jump magnitude $2p_i$ is to the true jump magnitude $2p_w$.

Comparing Fig. 5, *C* and *D*, it is obvious that the jump to the full level is detected faster than the jump to the sublevel. The alarm delay, the time from the jump to its detection, depends on the jump magnitude. Because the SHD decides about jump detection with the same reliability (Shirayev, 1961) irrespective of the jump magnitude, the alarm delay is not a general constant but is longer for smaller jumps where the signal-to-noise ratio is also smaller.

The alarm delay is important for describing the sensitivity of the SHD. If an isolated event is shorter than the alarm delay, it will not be detected. As a consequence, the temporal resolution t_{res} of the SHD is equal to the alarm delay. For noise-free events an equation for the alarm delay (equal to t_{res}) can be derived by dividing the threshold by the slope p_i^2 (Eq. 3) for the correct level.

$$t_{res,i} = \epsilon/p_i^2 \tag{8}$$

In this equation, the time resolution $t_{res,i}$ is given in sampling units. Note that t_{res} depends on the half jump magnitude p_i.

Illustration by a simulated example

We have simulated a 10-ms record of current through a patch with two different channels (Fig. 7 *A*). The small channel (7 pA) opens once at 2.2 ms and closes again at 7.8 ms. The other channel shows a flickering behavior with many short closures. It conducts a larger current, 10 pA. In Fig. 7 *B*, white background noise with a standard deviation of 2.0 pA is added. This noisy time series is processed by the SHD. Its output is shown in Fig. 7 *C*. Comparing Fig. 7, *A* and *C*, it becomes obvious that the reconstruction is nearly perfect. Only two short events are missed.

The diagnosis phase

In every patch-clamp setup the analog signal has to be passed through an antialiasing filter (AAF) before sampling because the frequencies above the half-sampling frequency have to be removed (sampling theorem, Blackman and Tukey, 1958). Normally, a four-pole or eight-pole Bessel filter is used as AAF. The consequence of low-pass filtering is sketched in Fig. 8. The originally rectangular edge is smoothed. Because of the soft transition from one level to another, the detection algorithm may be misled, because during the first sampling steps after the jump, the jump magnitude looks smaller than it actually is. Directly after the jump, the SHD as introduced above would be mistaken, diagnosing a small instead of a big jump.

The situation with the AAF is simulated in Fig. 7 *D*. In contrast to Fig. 7 *B*, the signal is passed through an eight-pole Bessel filter with a cutoff frequency of $f_{3dB} = 25$ kHz before sampling with 100 kHz (Fig. 7 *D*).

Fig. 7 *E* displays the signal reconstructed with the SHD. As expected, the SHD often comes to incorrect conclusions about the jump magnitude. Because the transitions are low-pass filtered, the SHD is often misled, diagnosing a closure $-s$ or an opening $+s$ instead of $-f$ or $+f$ (Fig. 7E). Some events, e.g., the closure at 5 ms, are long enough for the SHD to diagnose a second jump, which then goes to the correct level. This kind of transient error does not look too bad in the plot of the time series. But when doing statistics on how often what type of jump has occurred (see Figs. 10–12, below), this kind of temporarily false diagnoses, too, would lead to wrong results.

To develop an improved SHD that can be applied to filtered data, the basic algorithm is now modified. Instead of making the diagnosis immediately after jump detection, the SHD now goes on calculating the test values with the same actual level as before. The test values are processed according to Eq. 2 but without resetting any values below 0 or above ϵ. This diagnosis phase after jump detection lasts for $5 \cdot T_r$ with $T_r = 0.3321/f_{3dB}$ being the risetime (Colquhoun and Sigworth, 1983) of the AAF. Fig. 8 shows an example with our standard values for the sampling frequency $f_s = 100$ kHz and the filter cutoff frequency $f_{3dB} = 25$ kHz. The diagnosis phase is six sampling periods long. Including the sample of detection, it contains seven samples of each test value, marked by circles in Fig. 8. The improved SHD searches for the maximal test value during the diagnosis phase (the star in Fig. 8) and diagnoses a jump to the corresponding level.

Fig. 8 explains why this method leads to a correct diagnosis even in the case of filtered data. After the current signal has reached the new level, the slope of the correct test value is maximal in accordance with Eq. 3. From a certain time after the jump (some filter risetimes T_r) on, the diagnosis would be correct. During this diagnosis phase the correct test value wins over the incorrect test values. The duration 5 T_r for the diagnosis phase was determined "experimentally" by simulation. Several types of events with ratios of sublevel to full current I_s/I_f from 10% up to 90% were used. Trying different lengths of the diagnosis phase when analyzing the filtered events by the SHD confirms that a diagnosis phase of 5 T_r is long enough to overcome the AAF-induced problems.

There is, however, still an exception. Very short events like that in Fig. 9, where the opening is immediately followed by a closure, do not stay long enough at the new level for correct diagnosis. The short event shown in Fig. 9 would be diagnosed as a subconductance event. Therefore, the SHD is finally supplemented by the rule that events that are estimated to be shorter than five times the filter risetime (six

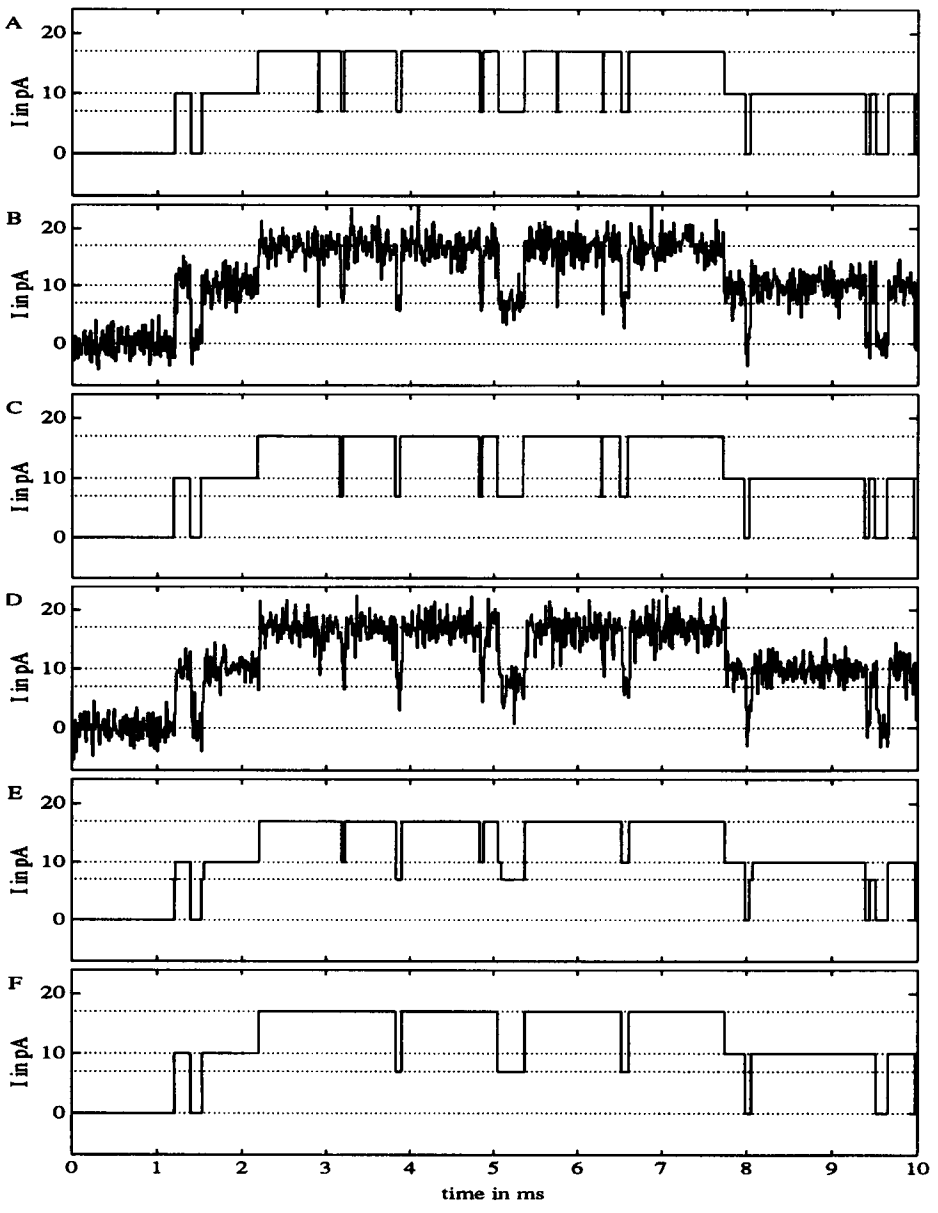

FIGURE 7 Simulation with and without AAF. There are two channels, a large one with 10 pA and a smaller one with 7 pA. The sampling interval is 10 μs. (*A*)Simulated time series (10 ms) of gating without noise. The signal switches between the four levels of current, indicated by horizontal dotted lines. It is the "original" for all following traces. (*B*) Time series of (A) with additional background noise σ = 2.0pA. The time series is not filtered. (*C*) Reconstruction by means of the basic SHD without diagnosis phase. The quality of reconstruction is good. (*D*) Simulated noisy time series with the same gating events as in (A). In contrast to (B), the time series is filtered through a Bessel low-pass filter with cutoff frequency f_{3dB} = 25 kHz. (*E*) Reconstruction with the basic SHD without diagnosis phase. The quality is unacceptable, because often the SHD has diagnosed a small instead of a big jump. (*F*) Reconstruction with the improved SHD, as developed in this article. The quality of the diagnoses is perfect. Some short events (e.g., at 2.9 or 5.8 ms) are ignored.

sampling steps or less in our case) are ignored. They are treated as if they were missed brief events. The question of missed events is addressed in the Discussion section.

Now we repeat the analysis of the simulated, filtered signal in Fig. 7 *D* and present the result in Fig. 7 *F*. In comparison with Fig. 7 *E*, more brief events are missed. But all detected events are assigned to the correct levels. This is the final version of the SHD for the analysis of patch-clamp data. It has also been used for the successful reconstruction of the measured data in Fig. 2.

GUIDELINES FOR APPLICATION

Length of diagnosis phase

The analog current signal from the patch-clamp amplifier is filtered through an antialiasing low-pass filter, commonly a Bessel filter. The frequency f_{3dB} of 3-dB attenuation of the AAF must be known to calculate the length of the diagnosis phase $5{\cdot}T_r = 1.66/f_{3dB}$. The length of the diagnosis phase is an empirical choice based on the criterion that the event amplitude is recognized correctly in subconductance data with $0.1 \le I_s/I_f \le 0.9$.

Determination of the current levels

For the cumulative-sum algorithm (Eq. 2) the following six parameters of the record have to be determined: 1) the current I_0 of the baseline (level $0f + 0s$), 2) the single-channel current I_f of a channel with big or full conductivity, 3) the single-channel current I_s of a subconductance level or a channel with small conductivity, 4) the maximum number of full channels N_f and 5) small channels N_s, and 6) the standard deviation σ of background noise.

We recommend an interactive eye-fit procedure consisting of two stages. First, the time series (e.g., Fig. 1 *A*) is displayed together with the levels $0f + 0s, \cdots, N_f f + N_s s$ of

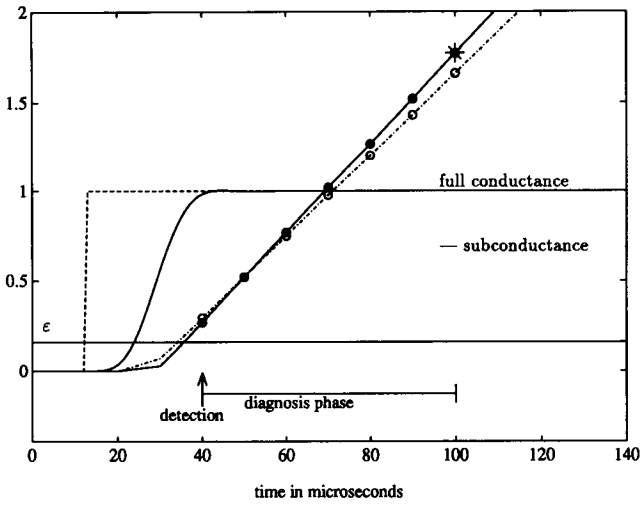

FIGURE 8 The diagnosis phase. This example shows that the diagnosis phase is required to make a correct decision because the current signal is prefiltered by an AAF, here a Bessel filter with f_{3dB} = 25 kHz. The unfiltered current jumps at time 12 μs from the baseline $0f + 0s$ to the full level $1f + 0s$ (dashed). The noise is 0. The sublevel is at 0.7 I_f (70% conductivity). The filtered current signal (solid) smoothly increases. Three sampling steps after the jump (time = 40 μs), when the filtered signal has not yet reached its full magnitude, the test values h_{1t} (solid, ●) for level $1f + 0s$ and h_{2t} (dash-dot, ○) for $0f + 1s$ have both exceeded the threshold $\epsilon = 0.1633\ I_f^2$. If the SHD would now have to decide about the jump magnitude, it would come to the incorrect result that a small jump to $0f + 1s$ had taken place, because the test value ○ for this level is still greater than the correct one ●. To avoid such misinterpretations caused by the AAF, the SHD waits with the decision until the end of the diagnosis phase. The test values within the diagnosis phase (○, ●) are compared. The maximum (star) is taken as an indication of the correct new level. (*Scales*) the current values in this plot are divided by the full current $I_f = 2p_1$ to show them in dimensionless form. The test values and the threshold ϵ are divided by I_f^2.

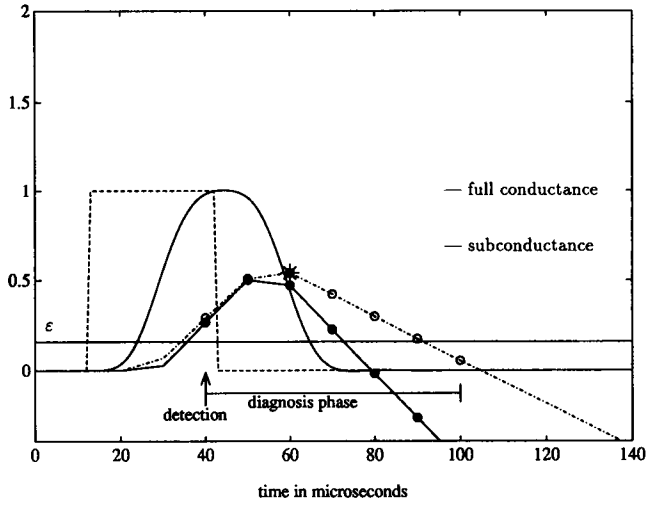

FIGURE 9 A very short open event (dashed), which is too short for a reliable determination of the magnitude. Its duration is 30 μs. The other parameters, the scales, and the meaning of the symbols are the same as in Fig. 8. The filtered current signal hardly reaches the level of full conductance. Therefore, the open event with full conductance looks similar to a subconductance event. The maximal test value during the diagnosis phase is marked by a star. It corresponds to a jump to the sublevel and therefore leads to an incorrect conclusion about the jump magnitude. The estimated length of the open event is 40 μs, the time between the last zero-valued test value at 20 μs and the maximum (star) at 60 μs. To avoid such misinterpretations, the estimated length is used to exclude too-short events with uncertain amplitude from further analysis. If the estimated event length is shorter than 5 T_r (filter risetime T_r = 13 μs), the event is simply ignored.

current as horizontal lines such as those in Fig. 7. It is now possible to change the parameters I_0, I_f, N_f, I_s, and N_s interactively until the fitted lines match the current levels of the record. In a second stage, the experimental amplitude histogram is displayed together with the levels of current as vertical lines (Fig. 1) and with the theoretical amplitude histogram (TAH I), which is a sum of gaussian distributions

$$\mathrm{TAH}(I) = \sum_{m=0}^{N_s} \sum_{n=0}^{N_f} a_{mn} \frac{1}{\sqrt{2\pi}\sigma} \times \exp\left(-\frac{1}{2}\left(\frac{I - (I_0 + mI_s + nI_f)}{\sigma}\right)^2\right). \quad (9)$$

The parameters a_{mn} are not adjusted manually; they are fitted by an automatic least-squares optimization to the measured amplitude histogram.

All the $(N_f + 1) \cdot (N_s + 1)$ levels in Eq. 9 are used for fitting and for the subsequent detection procedure with the SHD. These levels are sufficient to describe all possible levels of current in the signal. The question whether they are all needed leads to the more general issue of whether there are N_f big and N_s small channels acting independently or whether there are $N_f = N_s$ identical channels that can switch to a subconductance state with reduced current. The SHD is applied to the data without any restriction to one of these scenarios, but afterward the output of the SHD can be used to distinguish the subconductance case from the case of different channels.

DISTINGUISHING SUBLEVELS FROM DIFFERENT CHANNELS

The observation of different conductivities in single-channel data does not necessarily mean that there are channels with an additional conformation of reduced conductance. Different conductivities do also occur if channels in the patch are not identical and have different conductances. To find a method for distinguishing the "sublevel situation" from the "different channel situation" we simulate both kinds of data and compare the output of the SHD applied to both time series.

Simulation

We have chosen two gating schemes for simulation. One describes a flickering channel sometimes switching to a sublevel S with 70% conductivity. The scheme is shown at the left side in Fig. 10.

The other scheme (Fig. 11) comprises two distinct channels with different conductivity. The channel with the larger conductance has a flickering gating behavior, the small channel changes its conductance only about every 20 ms.

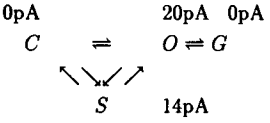

from \ to	0f + 0s	1f + 0s	2f + 0s	0f + 1s	1f + 1s	2f + 1s	0f + 2s	1f + 2s	2f + 2s
0f + 0s	–	590	0	5	0	0	0	0	0
1f + 0s	587	–	397	90	9	0	0	0	0
2f + 0s	0	400	–	0	58	0	0	0	0
0f + 1s	7	84	0	–	134	0	1	0	0
1f + 1s	0	9	61	131	–	0	15	0	0
2f + 1s	0	0	0	0	0	–	0	0	0
0f + 2s	0	0	0	1	15	0	–	0	0
1f + 2s	0	0	0	0	0	0	0	–	0
2f + 2s	0	0	0	0	0	0	0	0	–

FIGURE 10 Gating scheme of a channel with true subconductance state S and transition matrix obtained from a simulation with two channels, both according to the gating scheme. The rate constants are $k_{CO} = 10\ s^{-1}$, $k_{OC} = 5\ s^{-1}$, $k_{CS} = 2\ s^{-1}$, $k_{SC} = 3\ s^{-1}$, $k_{SO} = 300\ s^{-1}$, $k_{OS} = 100\ s^{-1}$, $k_{OG} = 1000\ s^{-1}$, and $k_{GO} = 5000\ s^{-1}$. The transition matrix on the right shows how many transitions there were between the various levels the SHD has counted in the reconstructed record. The dashed boxes frame the transitions $f \rightarrow s$ and $s \rightarrow f$ between full and sublevel. The solid boxes surround the levels with more than two channels open. Because there are only two channels simulated, the solid boxes remain empty.

The simulation procedure is described in detail in a previous article (Draber and Schultze, 1994). The main features are 1) simulation in discrete time with a simulation period of $T_{sim} = 1\ \mu s$, which is short enough with respect to the lifetimes of the states of the two models and with respect to the risetime of the AAF; 2) at every simulation step the transition probabilities $T_{sim}k_{ij}$ from the actual state i to the other states $j \neq i$ and the probability $1 - \sum_j T_{sim}k_{ij}$ to stay in state i provide the basis for a Monte Carlo simulation; 3) the typical colored noise of a patch-clamp setup is added. Its power spectrum is flat below 1 kHz and rises proportionally to the frequency above 1 kHz (Colquhoun and Sigworth, 1983; Schultze and Draber, 1993); 4) to simulate the electronic processing of the measured data, an eighth-order Bessel filter with a cutoff frequency (−3 dB) of $f_{3dB} = 25$ kHz is used as a low-pass filter for antialiasing; and 5) sampling with 100 kHz as it is done in our laboratory setup (Schultze and Draber, 1993; Draber et al., 1993; Draber and Schultze, 1994) is the final step of simulation.

The simulated records have a length of 2 s and contain 200,000 sampled values; the standard deviation of noise is $\sigma = 2.0$pA. One time series represents the behavior of two small channels and two large channels according to the gating scheme in Fig. 11. In contrast, the other time series was obtained by simulating two identical channels with subconductance levels (see gating scheme in Fig. 10).

Transition matrix

The rows and columns of the transition matrix correspond to the levels of current. The rows stand for the level before a transition, and the columns stand for the level afterward. Every time the SHD detects a jump, it increments the corresponding element in the matrix. Finally, the matrix gives the number of transitions between the levels. Note that the transition matrices in Figs. 10 and 11 are nearly symmetrical. This is a consequence of the microreversibility of the underlying gating schemes.

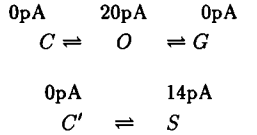

from \ to	0f + 0s	1f + 0s	2f + 0s	0f + 1s	1f + 1s	2f + 1s	0f + 2s	1f + 2s	2f + 2s
0f + 0s	–	221	0	11	0	0	0	0	0
1f + 0s	224	–	193	3	34	0	0	0	0
2f + 0s	0	186	–	0	6	21	0	0	0
0f + 1s	7	8	0	–	326	0	3	0	0
1f + 1s	0	40	5	323	–	368	1	25	0
2f + 1s	0	0	15	0	367	–	0	3	20
0f + 2s	0	0	0	7	2	0	–	152	0
1f + 2s	0	0	0	0	27	7	157	–	112
2f + 2s	0	0	0	0	0	9	0	123	–

FIGURE 11 Transition matrix obtained from data simulated according to the gating schemes on the left with two large and two small channels. The rate constants of the simulated model are $k_{CO} = 10\ s^{-1}$, $k_{OC} = 5\ s^{-1}$, $k_{OG} = 1000\ s^{-1}$, $k_{GO} = 5000\ s^{-1}$, $k_{C'S} = 40\ s^{-1}$, and $k_{SC'} = 60\ s^{-1}$. Detected transitions $f \rightarrow s$ and $s \rightarrow f$ in the dashed boxes are rare because they are not produced by the gating scheme. Such transitions are mimicked by coincidental transitions $+f$ and $-s$ or $-f$ and $+s$ occurring in the same sampling interval. The solid boxes contain the quite frequent transitions to levels with more than two channels open.

The transition matrix turns out to be a useful tool for the decision whether the channels have a subconductance conformation or if there are simply several channels of different conductivity within the patch. In the "different channel situation" the transitions $f \rightarrow s$ and $s \rightarrow f$ in the dashed boxes are very unlikely. Of course, such transitions may be mimicked by coincidental transitions of a small and a large channel. $+f$ and $-s$ together at the same time look like a $s \rightarrow f$ transition. Nevertheless, the "different-channel situation" is characterized by only small numbers in the dashed boxes of the transition matrix (Fig. 11). In the "sublevel situation" with $N = N_f = N_s$ on the other hand, transitions to levels with more than N channels open are strictly forbidden. This situation is characterized in Fig. 10 by zeroes in the solid frames.

With these rules as the basis for a distinction between the two principally different situations, we come back to the measurement shown in Fig. 1. The transition matrix in Fig. 12 is the result of the SHD applied to the measured data in Fig. 1. It also shows symmetry. There are no transitions with more than one channel involved. The solid frame is empty. The dashed boxes, however, report 333 transitions $f \rightarrow s$ and $s \rightarrow f$. The numbers in the transition matrix (Fig. 12) allow the conclusion that the observed K^+ channel in the tonoplast of *Chara corallina* can switch to a conformation with reduced conductivity.

DISCUSSION

Required accuracy of levels

The SHD uses the information about the levels as prior knowledge. In noisy data, the determination of these levels by means of an eye fit is not always accurate. The question arises how large deviations between true and fitted level can be tolerated by the SHD. From the parabola in Fig. 6 it becomes clear that at least one condition must be fulfilled. Given that the SHD chooses the level closest to the true one, the fitted correct level must be nearer to the true level in the data than any other alternative level.

If the number of channels is high and the open probability is low, a reliable determination of the number N of channels is not always possible. Statistical tests (Horn, 1991; Draber et al., 1993) might be a useful help, but they, too, are more complicated in the case of different channel types. If the number of channels is not determined correctly, this has consequences on the interpretation of the transition matrix for the distinction between different channels and channels with sublevels. High numbers in the solid frames (Fig. 11) may not only be due to independent small and large channels, they may simply be due to an underestimation of the channel number. Conversely, if the channel number is overestimated, the solid boxes remain empty even if there are channels of different type.

Therefore, the distinction between the "sublevel situation" and the "different channel situation" should be based mainly on the numbers in the dashed boxes if the number of channels is not precisely known.

from \ to	$0f+0s$	$1f+0s$	$0f+1s$	$1f+1s$
$0f+0s$	–	67	15	0
$1f+0s$	71	–	164	0
$0f+1s$	10	169	–	0
$1f+1s$	0	0	0	–

FIGURE 12 Transition matrix obtained from the measurement on *Chara* K^+ channels shown in Fig. 1. The two dashed boxes contain the transitions $f \rightarrow s$ and $s \rightarrow f$ between full and sublevel. The solid frame surrounds the levels with more than one channel open. Because there are many (333) transitions between full and sublevel and no events with more than one open channel, this is evidence of a subconductance conformation of the K^+ channel in the *Chara* tonoplast.

Missed events

If dwell-time distributions are analyzed, the effect of missed events has to be taken into account. In contrast to equidistant levels, where the omission of brief events (Colquhoun and Sigworth, 1983; Ball et al., 1993; Draber and Schultze, 1994) can be described by a single parameter, the time resolution t_{res}, the situation here is more complex.

Analyzing single-channel data with sublevels, the temporal resolution is no longer a constant (see Eq. 8). Jumps are detected earlier if they have a larger magnitude. This feature of the SHD becomes very obvious in Fig. 5 where it takes nine sampling intervals to detect a jump to the sublevel, but only four for the detection of a jump to the full level. A sublevel event of eight sampling steps duration would not have been detected, whereas a full-conductance event of the same duration would, no doubt, be detected.

Besides this jump magnitude-dependent resolution limit, there is another fixed dead time of the detector caused by the AAF that has forced us to introduce the diagnosis phase. All events shorter than $5 \cdot T_r$ are ignored, because their magnitude cannot be determined exactly. This imposes a lower bound on the temporal resolution, especially for larger jump magnitudes.

Because of this combination of two criteria for omission of short events, the development of a method for missed events correction is expected to be much more difficult than for the standard case with equidistant levels.

Computing time

The complexity of the mathematical calculations (Eq. 2) is similar to conventional detectors for equidistant levels, e.g., a Bessel filter with threshold detection. On a 486 personal computer with 50-MHz clock frequency, it takes 40 s to analyze a record with 200,000 samples, including already the creation of the reconstructed time series, of the transition matrix, and of dwell-time histograms. The SHD needs about the same computing time as other recursive detectors, but it is the only one that can analyze subconductance data.

Generalization

The description above was restricted to records with two different unitary conductances. It is obvious that the algorithm can be extended to records with an arbitrary number of sublevels or channel types just by the correct selection of the half jump magnitudes p_i.

We thank Dr. U.-P. Hansen for his continuous support during the investigations and for critical reading. We also thank Dr. Christian Ruge for helpful discussions.

REFERENCES

Ball, F. G., G. F. Yeo, R. K. Milne, R. O. Edeson, B. W. Madsen, and M. S. P. Sansom. 1993. Single ion channel models incorporating aggregation and time interval omission. *Biophys. J.* 64:357–374.

Basseville, M., and A. Benveniste, editors. 1986. Detection of Abrupt Changes in Signals and Dynamical Systems. Springer-Verlag, New York.

Blackman, R. B., and J. W. Tukey. 1958. The Measurement of Power Spectra, Dover Publications, New York.

Chung, S. H., J. B. Moore, L. Xia, L. S. Premkumar, and P. W. Gage. 1990. Characterization of single channel currents using digital signal processing techniques based on hidden Markov models. *Philos. Trans. R. Soc. Lond. B Biol. Sci.* 329:265–285.

Colquhoun, D., and F. J. Sigworth. 1983. Fitting and statistical analysis of single channel records. *In* Single-Channel Recording. B. Sakmann, and E. Neher, editors. Plenum Press, New York, London. 191–263.

Draber, S., R. Schultze, and U.-P. Hansen. 1993. Cooperative behavior of K^+ channels in the tonoplast of *Chara corallina*. *Biophys. J.* 65: 1553–1559.

Draber, S., and R. Schultze. 1994. Correction for missed events based on a realistic model of a detector. *Biophys. J.* 66:191–201.

Ferguson, W. B., O. B. McManus, and K. L. Magleby. 1993. Opening and closing transitions for BK channels often occur in two steps via sojourns through a brief lifetime subconductance state. *Biophys. J.* 65:702–714.

Hinkley, D. V. 1971. Inference about the change-point from cumulative-sum-tests. *Biometrika.* 57:1–17.

Horn, R. 1991. Estimating the number of channels in patch recordings. *Biophys. J.* 60:433–439.

Page, E. S. 1955. A test for a change in parameter occurring at an unknown point. *Biometrika.* 42:523–527.

Patlak, J. B. 1988. Sodium channel subconductance levels measured with a new mean-variance analysis. *J. Gen. Physiol.* 92:413–430.

Patlak, J. B. 1993. Measuring kinetics of complex single ion channel data using mean-variance histograms. *Biophys. J.* 65:29–42.

Ramanan, S. V., and P. R. Brink. 1993. Multichannel recordings from membranes which contain gap junctions. II. Substates and Conductance Shifts. *Biophys. J.* 65:1387–1395.

Schild, L., A. Ravindran, and E. Moczydlowski. 1991. Zn^{2+}-induced subconductance events in cardiac Na^+ channels prolonged by batrachotoxin. *J. Gen. Physiol.* 97:117–142.

Schultze, R. 1992. Robust identification for adaptive control: the dynamic Hinkley-detector. *In* Proceedings of the Fourth IFAC Symposium on Adaptive Systems in Control and Signal Processing. July 1–3, 1992, Grenoble, France. Pergamon Press. 23–28.

Schultze, R. 1993. Robust identification for adaptive control: the dynamic Hinkley-detector is superior to RLS. *In* Proceedings of the Second European Control Conference 1993, June 28–July 1, 1993, Groningen, The Netherlands, 4:2197–2202.

Schultze, R., and S. Draber. 1993. A nonlinear filter algorithm for the detection of jumps in patch-clamp data. *J. Membr. Biol.* 132:41–52.

Shirayev, A. N. 1961. The problem of the most rapid detection of a disturbance in a stationary process. *Soviet Math. Dokl.* 2:795–799.

Tyerman, S. D., B. R. Terry, and G. P. Findley. 1992. Multiple conductances in the large K^+ channel from *Chara corallina* shown by a transient analysis method. *Biophys. J.* 61:736–749.